Assessing phonon coherence using spectroscopy

Zhongwei Zhang,[1] Yangyu Guo,[2] Marc Bescond,[3] Masahiro Nomura,[4] Sebastian Volz,[1,5,*] and Jie Chen[1,†]

[1]*Center for Phononics and Thermal Energy Science, School of Physics Science and Engineering and China-EU Joint Laboratory for Nanophononics, Tongji University, Shanghai 200092, People's Republic of China*

[2]*Institut Lumière Matière, Université Claude Bernard Lyon 1-CNRS, Université de Lyon, Villeurbanne 69622, France*

[3]*IM2NP, UMR CNRS 7334, Aix-Marseille Université, Faculté des Sciences de Saint Jérôme, Case 142, 13397 Marseille Cedex 20, France*

[4]*Institute of Industrial Science, The University of Tokyo, Tokyo 153-8505, Japan*

[5]*Laboratory for Integrated Micro and Mechatronic Systems, CNRS-IIS UMI 2820, The University of Tokyo, Tokyo 153-8505, Japan*

(Received 25 June 2022; revised 11 April 2023; accepted 12 April 2023; published 24 April 2023)

As a fundamental physical quantity of thermal phonons, temporal coherence participates in a broad range of thermal and phononic processes, while a clear methodology for the measurement of phonon coherence is still lacking. In this paper, we derive a theoretical model for the experimental exploration of phonon coherence based on spectroscopy, which is then validated by comparing Brillouin light scattering data and direct molecular dynamic simulations of confined modes in nanostructures. The proposed model highlights that confined modes exhibit a pronounced wavelike behavior characterized by a higher ratio of coherence time to lifetime. The dependence of phonon coherence on system size is also demonstrated from the spectroscopy data. The proposed theory allows for reassessing the data of conventional spectroscopy to yield coherence times, which are essential for the understanding and the estimation of phonon characteristics and heat transport in solids in general.

DOI: 10.1103/PhysRevB.107.155426

I. INTRODUCTION

Coherence is a fundamental characteristic of the wavelike behavior of elementary particles and quasiparticles [1–4]. Due to the wave nature of lattice vibrations, phonon coherence has been established as the dominant source of various unique thermal transport phenomena, such as coherent thermal transport (including minimum thermal conductivity in nanophononic crystals [1,2,5–8] and phonon Anderson localization in disordered nanophononic crystals [9–13]), band folding [5,14,15], and phonon confinement [16–18]. Furthermore, recent studies [19–23] have uncovered the significant impact of phonon coherence on phonon-phonon scattering [19–21], phonon modal correlations [20,22,23], and interfacial phonon propagation [12], leading to clear discrepancies with the predictions obtained from the particle picture and also to promote coherence as a critical phonon attribute.

Phonon coherence is usually quantified by the physical quantity of coherence time [24]. However, most of the experimental demonstrations of coherence for thermal phonons are qualitatively inferred from the variation of measured thermal conductivity [1,2,10,25]. For instance, the existence of coherent phonons is indirectly evidenced by the experimental observation of the nonmonotonic variation of superlattice thermal conductivity with decreasing superlattice period [2]. On the other hand, phononic quantities, including phonon number, eigenfrequency, and scattering rate, can be measured from the well-established time-domain thermoreflectance approach [26–28] or various spectroscopies [29–34], which are boosting the exploration of phonon physics and thermal transport in different matters. Clearly, the experimental characterization of the coherence of thermal phonons is lagging behind, due to the lack of an adequate theory, which impedes the scientific understanding and practical application of phonon physics and thermal transport.

In this paper, we develop a theoretical model for experimentally investigating phonon coherence using spectroscopy measurements. The predictions of the model disclose that in the case of confined nanostructures, such as nanowires (NWs) and nanomembranes (NMs), the coherence time for different modes can be efficiently extracted. Because of the substantial phonon confinement, modes have a prominent wavelike characteristic and exhibit a significant dimensionality-dependent coherence [17,35,36]. Furthermore, the phonon coherence times and lifetimes detected from spectroscopy agree qualitatively well with the outcomes from the direct molecular dynamic (MD) simulations. The proposed theory reassesses mainstream spectroscopies to quantify mode coherence having a general impact on the understanding and the estimation of phonon and thermal properties.

II. THEORY DEVELOPMENT

Phonon lifetime is conventionally measured from the Lorentzian fitting of experimental spectra, such as inelastic neutron scattering, inelastic x-ray scattering, and Brillouin-Mandelstam light scattering [17,32,37–39]. The underlying physics of a Lorentzian fit is based on the hypothesis of an exponential decay of phonon dynamics in time, assuming phonons as particles governed by diverse scattering processes [40,41]. In the frequency domain, the Lorentzian function is expressed as [40,42,43]

$$\Phi_{\mathbf{k}s}(\omega) = \frac{I_0}{4(\omega - \omega_{\mathbf{k}s})^2 {\tau_{\mathbf{k}s}^p}^2 + 1}, \tag{1}$$

*volz@iis.u-tokyo.ac.jp
†jie@tongji.edu.cn

where $\Phi_{\mathbf{k}s}(\omega)$ is the spectral mode energy and I_0 is the peak intensity. The physical quantities of eigenfrequency ($\omega_{\mathbf{k}s}$) and lifetime ($\tau^p_{\mathbf{k}s}$) are simultaneously evaluated by matching the experimental measurements as implemented in Refs. [17,32]. Equation (1) can also be expressed in terms of the modal linewidth ($\gamma_{\mathbf{k}s}$) according to the expression of $\tau^p_{\mathbf{k}s} = \frac{1}{2\gamma_{\mathbf{k}s}}$. Using the normal mode decomposition method, the spectral energy $\Phi_{\mathbf{k}s}(\omega)$ can also be calculated from MD simulations, making Eq. (1) a widely used model for studying the phonon lifetimes and thermal transport in theoretical and numerical simulation works [40,43–46].

Recent studies [21,23,47] demonstrated the significance of coherence on the phonon dynamics and thermal transport in various solids. By taking into account the coherence effects, a previous work [21] established that the time-dependent phonon number should be corrected as follows,

$$N_{\mathbf{k}s}(t) = N_{\mathbf{k}s}(0)e^{-\gamma'_{\mathbf{k}s}t}e^{-4\ln 2\cdot\Omega^2_{\mathbf{k}s}t^2}, \tag{2}$$

where $N_{\mathbf{k}s}(0)$ denotes the phonon number of mode $\mathbf{k}s$ at the initial time of decay. γ' represents the corrected linewidth for this mode and $\Omega_{\mathbf{k}s}$ denotes the inverse of the temporal extension of the wave packet. The temporal extension of phonon wave packets is an intrinsic characteristic of materials that arises from the interference between different lattice waves [48,49], which should differ from the one of the laser-excited photons. The corrected phonon lifetime from Eq. (2) writes $\tau^{p'}_{\mathbf{k}s} = \frac{1}{2\gamma'_{\mathbf{k}s}}$ and the temporal coherence time $\tau^c_{\mathbf{k}s} = \frac{1}{\Omega_{\mathbf{k}s}}$. $\tau^{p'}_{\mathbf{k}s}$ describes the particlelike behavior of phonons as for instance the scattering processes introduced by Boltzmann transport theory and the phonon-gas model, which assume the existence of phonon particles. However, phonon particles are in fact spatially and temporally localized vibrational waves. $\tau^c_{\mathbf{k}s}$ assesses this wavelike behavior via its in-phase extension.

On the other hand, the phonon number can also be defined from the normal mode coordinate $q_{\mathbf{k}s}$ (see Sec. S1 in the Supplemental Material [50] for a definition) as

$$N_{\mathbf{k}s}(t)\hbar\omega_{\mathbf{k}s} = \tfrac{1}{2}\dot{q}_{\mathbf{k}s}(t)\dot{q}^*_{\mathbf{k}s}(t) + \tfrac{1}{2}\omega^2_{\mathbf{k}s}q_{\mathbf{k}s}(t)q^*_{\mathbf{k}s}(t), \tag{3}$$

where $*$ indicates the complex conjugate. Based on Eqs. (2) and (3), we can further infer the expression of the normal mode coordinate as [24]

$$q_{\mathbf{k}s}(t) \approx q_0 e^{-i\omega_{\mathbf{k}s}t}e^{-\frac{\gamma'_{\mathbf{k}s}}{2}t}e^{-2\ln 2\cdot\Omega^2_{\mathbf{k}s}t^2}, \tag{4}$$

where q_0 denotes the amplitude and $e^{-i\omega_{\mathbf{k}s}t}$ corresponds to the natural oscillation of the lattice wave. The approximation assumes that the normal mode coordinate and velocity have the same decay trend. In a further step, the mode energy can be obtained from the Fourier transform of Eq. (4) as

$$\Phi_{\mathbf{k}s}(\omega) = 2\times\frac{1}{2}\omega^2_{\mathbf{k}s}\left|\int_0^\infty q_{\mathbf{k}s}(t)e^{i\omega t}dt\right|^2. \tag{5}$$

The coefficient 2 accounts for the summation of the kinetic and the potential terms at thermodynamic equilibrium. Our derivation in Sec. S2.1 of the Supplemental Material [50] shows that the obtained model of mode energy contains a term of time integral, which is complex to perform the spectroscopy fitting, while the spectroscopy model that includes both lifetime and coherence time can be approximated to (see Sec. S2 for complete derivation and approximation)

$$\Phi_{\mathbf{k}s}(\omega) \approx I\cos\left[\frac{1}{16\ln 2}\frac{\tau^{c2}_{\mathbf{k}s}}{\tau^{p'}_{\mathbf{k}s}}(\omega-\omega_{\mathbf{k}s})\right]e^{\frac{-(\omega-\omega_{\mathbf{k}s})^2\tau^{c2}_{\mathbf{k}s}}{8\ln 2}}, \tag{6}$$

where I denotes the peak intensity. In contrast to the Lorentzian model of Eq. (1), our theory can simultaneously provide the information of eigenfrequency ($\omega_{\mathbf{k}s}$), coherence corrected phonon lifetime ($\tau^{p'}_{\mathbf{k}s}$), and coherence time ($\tau^c_{\mathbf{k}s}$). In addition, a detailed discussion and comparison of the accuracy and efficiency with different models, i.e., the original model [before approximation and with an integral in Eq. (S4) or (S8)] and the approximated model [Eq. (6)], is presented in Sec. S2.2. The approximated model is shown to have a high accuracy and efficiency, demonstrating its dependability in the subsequent results.

As previously discussed, the spectral energy can be measured by experimental spectroscopy as implemented by many different techniques, and can also be calculated from the normal mode decomposition with inputs from MD simulations. However, Eq. (6) reveals that $\tau^{p'}_{\mathbf{k}s}$ and $\tau^c_{\mathbf{k}s}$ are coupled in the spectral domain, making the fitting for these two quantities nonunique.

A previous study [21] showed that the lifetimes fitted by Eq. (1) are close to the coherence corrected ones, i.e., $\tau^p_{\mathbf{k}s} \approx \tau^{p'}_{\mathbf{k}s}$. Following this approximation, the lifetimes and coherence times can be estimated from the spectral energy via a two-step fitting: (1) the lifetime and eigenfrequency can be obtained by fitting the spectral energy with Eq. (1); (2) the second fitting is performed to extract the coherence time from Eq. (6) based on (1). The fitting code has been implemented in our open-source WPPT package [51], which was originally designed to study the coherence of phonons and the thermal conductivity of solids.

III. THEORY APPLICATION

A. Coherence time

To support the proposed model, we further investigate the coherence of phonons in the confined nanostructures. Previous studies [16–18,52,53] demonstrated that phonon confinement appears along the nonperiodic direction as reducing the structure dimensionality to one or two. In one-dimensional NWs, for example, phonons are confined in the diameter direction as standing waves and exhibit a diameter-dependent confinement [17,27,54]. For instance, Kargar *et al.* [17] have measured the phonon subbands in GaAs NWs using Brillouin-Mandelstam light scattering spectroscopy. Figure 1(a) reports the experimental spectrum from Ref. [17] at a specific wave vector for a GaAs NW with a diameter $D = 122$ nm. Peaks corresponding to different phonon modes clearly appear. The fitting of a specific mode is shown in Fig. 1(b). The proposed model displays a better agreement with the spectroscopy data than does the Lorentzian fit. The fitting errors predicted by the two models are further evaluated with the mean square error (MSE). The results of

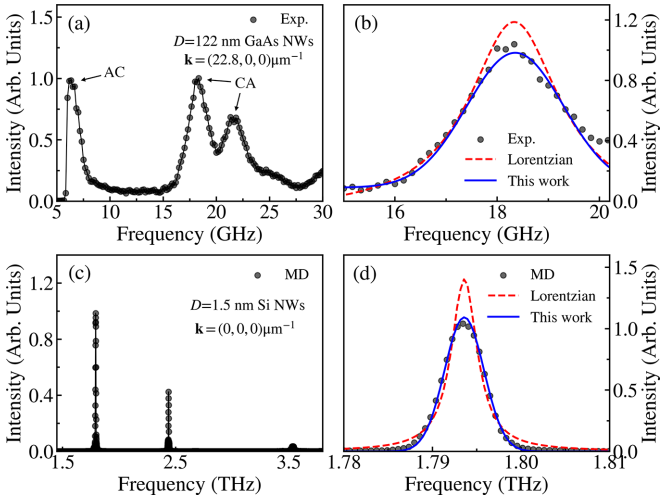

FIG. 1. (a) The experimental spectrum of GaAs nanowires with a diameter $D = 122$ nm and interdistance 700 nm at the specific wave vector $\mathbf{k} = (22.8, 0, 0)$ μm^{-1}. Different modes are labeled. Replotted from data in Ref. [17] by Kargar *et al.* (b) The fitting of experimental spectroscopy data with the classical Lorentzian model of Eq. (1) and the proposed one in Eq. (6) after subtracting the background to ensure a decay to zero. (c) The MD spectral analysis of Si nanowires with a diameter $D = 1.5$ nm at the specific wave vector $\mathbf{k} = (0, 0, 0)$ μm^{-1}. (d) The fitting of the MD calculated spectral energy with the classical Lorentzian model of Eq. (1) and the one of Eq. (6).

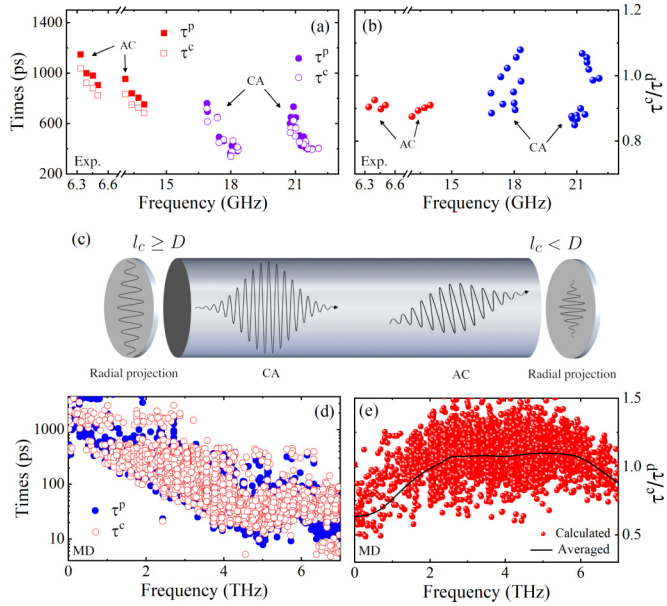

FIG. 2. (a) The estimated lifetimes (τ^p) and coherence times (τ^c) vs frequency obtained from the experimental spectroscopy of GaAs NWs with diameter $D = 122$ nm. (b) The ratio τ^c/τ^p vs frequency for GaAs NWs. The AC and CA in (a) and (b) denote normal acoustic and confined acoustic modes, respectively. (c) A schematic of the different behaviors of AC and CA modes in NWs. l_c is the size of the phonon wave packet along the radial direction. D refers to the nonperiodic (diameter) dimension of NWs. (d) The estimated lifetimes (τ^p) and coherence times (τ^c) vs frequency obtained from the MD spectral energy of Si NWs with diameter $D = 1.5$ nm. (e) The ratio τ^c/τ^p vs frequency for Si NWs. The huge number of data in (d) and (e) is originating from the dense phonon branches and the numerous wave vectors accessed in MD simulations. The line in (e) corresponds to the averaged ratio at a given frequency with an interval of 0.6 THz.

MSEs indicate that the proposed model improves the fitting of the spectroscopy data in general by including the phonon coherence (see Secs. S4.1 and S4.2 in the Supplemental Material [50] for details).

To provide further comparison, we also calculate the spectral energy of Si NWs with smaller diameters, from MD simulations. The details about MD simulations and the normal mode decomposition [55,56] are provided in the Supplemental Material [50]. Figure 1(c) reports the spectral energy at wave vector $\mathbf{k} = (0, 0, 0)$ for a Si NW with a diameter $D = 1.5$ nm. The fitting is carried out for a specific mode in Fig. 1(d) and the proposed model was found to provide a high accuracy as found in the experimental spectroscopy data of Fig. 1(b), when the coherence effects are considered in the full phonon dynamics. The same model is also applied to study the phonon coherence in two-dimensional Si NMs with the measured Raman scattering spectroscopy [18], as reported in Sec. S6 of the Supplemental Material [50]. Additionally, the estimated MSEs for the Si NWs and NMs are also discussed in Secs. S4.3 and S4.4. Lower values of MSEs are also found for the proposed model in the systems with stronger phonon coherence. Although other factors may produce artificial broadening in spectroscopy measurements [57], the reasonable fitting with the results from MD simulations still suggest the accessibility of the proposed model.

After validating the theoretical model with individual mode fittings, we then study the variation of phonon lifetimes and coherence times from different dependences. The estimated phonon lifetimes and coherence times of GaAs NWs are reported in Figs. 2(a) and 2(b), respectively, which are obtained from the experimental spectroscopy at different wave vectors. The fitting details of different acoustic modes are presented in Sec. S5 of the Supplemental Material [50]. Lifetimes and coherence times are always close to each other and gradually decrease when frequency increases, which agrees qualitatively well with the general frequency dependence observed in various solids [21,23,44,47]. The acoustic (AC) modes have higher characteristic times than those of confined acoustic (CA) modes at high frequencies [see the identification of different modes in Figs. 1(a) and S6].

We further evaluate the coherence of different modes through the ratio of coherence times to lifetimes, τ^c/τ^p. This ratio compares the degree of the wavelike behavior to the particlelike one for a specific mode. Figure 2(b) highlights that when comparing the acoustic modes to the confined ones, the wavelike behavior of phonons gradually intensifies. As experimentally confirmed by Kargar *et al.* [17], those GaAs NWs modes are resulting from a confinement effect, which clearly exhibits a more pronounced coherence as compared to the bulk optical and the low-frequency AC modes. For CA modes, the size of the phonon wave packets, i.e., the spatial coherence length of phonons l_c [23,58], along the radial direction is comparable to or even larger than the nonperiodic dimension of nanostructures, as indicated in Fig. 2(c), which

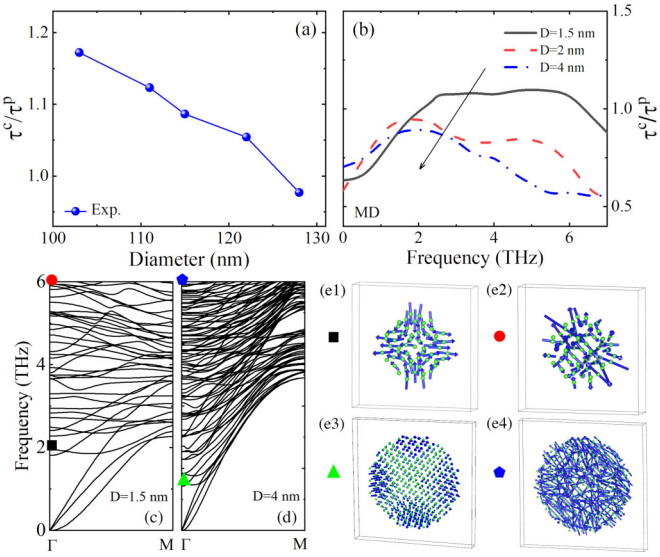

FIG. 3. (a) The ratio τ^c/τ^p vs diameter for the confined mode of lowest frequency in GaAs NWs is based on the spectroscopy data from Ref. [17]. (b) The average ratio τ^c/τ^p vs frequency for Si NWs with different diameters. The arrow in (b) denotes an increasing trend with diameter. Phonon dispersion of Si NWs with diameters $D = 1.5$ nm (c) and $D = 4$ nm (d). (e1)–(e4) Perspective views of the atomic eigendisplacements that correspond to the specific modes in (c) and (d) referred to as symbols. Arrows in (e1)–(e4) denote the atomic vibrational directions.

results in the fact that phonon modes are confined along the diameter direction as continuous waves with strong phonon coherence. Contrastively, the wave packets of AC modes can tilt along any direction and their l_c along the radial direction are always much smaller than the size of the nonperiodic dimension D, i.e., $l_c < D$, causing the dominant particle picture for the phonon wave packets of those modes.

A further implementation of the proposed model to MD simulations is presented in Figs. 2(d) and 2(e). The decreasing trend of phonon lifetimes and coherence times as a function of frequency in the full Brillouin zone is also obtained in Si NWs as a first validation. For phonons with frequencies below 2 THz, where the acoustic modes are predominant [see Fig. 3(c)], the values of τ^c/τ^p exhibit an increasing trend with frequency, indicating the enhanced coherence as approaching to the confined mode frequency. This outcome qualitatively agrees with the results from the experimental spectroscopy of GaAs NWs.

Note that the full phonon dispersion in Fig. 3(c) contains a large range of modes which yields the scattered data of Fig. 2(e). The average (black line, averaged over frequency) clearly discloses the enhanced wavelike behavior for confined modes in the middle frequency range. In addition, at frequencies above 6 THz, the ratio decreases with frequency, demonstrating that the high-frequency bulklike optical phonons are involved in scattering events resulting in a significant phase destruction and smaller phonon wave packets.

The phonon confinement effect weakens when the size in the confined direction increases, i.e., when the diameter and thickness increase in NWs and NMs, respectively. The weakened confinement due to a larger system size is also accompanied by a frequency reduction of the confined modes as observed in spectroscopy measurements [17,18] and phonon dispersions of Figs. 3(c) and 3(d).

With the spectroscopy data of the GaAs NWs from Ref. [17], we further estimate the dependence of the wavelike behavior on the diameter from the ratio τ^c/τ^p. Figure 3(a) reports the decrease of the ratio τ^c/τ^p with increasing diameter for a confined mode, indicating the suppressed wavelike behaviors due to the weakened phonon confinement effect. The suppressed wavelike behavior and phonon confinement with increasing thickness are also observed in two-dimensional Si NMs (see Sec. S6 in Supplemental Material [50]). Obviously, in the larger sized NWs and NMs, the coherence length of confined phonon modes becomes smaller than the nonperiodic dimension. The phonon confinement is correspondingly weakened and phonons are colliding with boundaries as particles, yielding to a decoherence mechanism [see Fig. 2(c)].

We further study the size-dependent wavelike behavior using the MD spectral energy. Figure 3(b) highlights a pronounced impact of the diameter on the times ratio in Si NWs. The increase of τ^c/τ^p below 2 THz is shifted to a lower frequency as increasing the diameter due to the redshift of the confined mode frequency [see Figs. 3(c) and 3(d)]. Besides the suppressed wavelike behavior around the frequency of the confined modes, a larger diameter substantially reduces this ratio in the high-frequency range, which might be caused by the stronger boundary scattering in the studied diameter size as phonons behave more as particles [59] in which τ^c and τ^p should be simultaneously reduced.

B. The origin of coherence

To demonstrate the phonon coherence assessed by the proposed model, we further investigate the modal wave information of Si NWs from lattice dynamics calculations [60] in Figs. 3(c)–3(e). Figures 3(c) and 3(d) indicate that the confined modes around the region of lowest optical modes shift to lower frequencies as the diameter increases from 1.5 to 4 nm. In Fig. 3(e), we further compare the eigendisplacements of two kinds of optical modes at different frequencies [see the symbols in Figs. 3(c) and 3(d)], i.e., the confined acoustic modes in the low-frequency region with high coherence, and the bulk optical modes with strong particlelike behavior. The eigendisplacements of the confined modes of the ultrathin NWs (i.e., $D = 1.5$ nm) reveal a strong collective confinement effect [see Fig. 3(e1)], in which the atoms at the four corners are collectively vibrating in phase and clearly collide with the boundary (see Video 1 in the Supplemental Material). However, for the $D = 4$ nm NWs reported in Fig. 3(e3), the in-phase vibrations of the NW lattice cell are still maintained but the collision with the boundary has been partially suppressed (see Video 2 in the Supplemental Material), resulting in a weakened confinement effect. The reduced wavelike behaviors expressed by the eigendisplacements are well consistent with the estimated lifetimes and coherence times. Although the lifetimes and coherence times are still on the same order of magnitude, the estimated coherence degree is critical to further understand the coherent thermal transport in nanophononic crystals [1,9–11] as well

as interband coherence in complex crystals and amorphous materials [19,20,22,23].

On the other hand, the eigendisplacements of the bulk optical modes are also shown in Figs. 3(e2) and 3(e4). Random and disordered vibrations are found for these optical modes which are located in the high-frequency region of the phonon dispersion. These vibrations with out-of-phase atomic oscillations indicate the weak wavelike behaviors as predicted by the proposed model in Figs. 2(e) and 3(b) (see Videos 3 and 4 in the Supplemental Material).

IV. CONCLUSION

Our proposed model delivers a description of phonon coherence and provides the measurable physical quantity of coherence time using conventional phonon spectroscopy. In the context of previous studies on confined nanostructures, our proposed model has demonstrated its general applicability in assessing the phonon coherence from both experimental measurements and numerical simulations. As a general framework, the developed model is an effective approach for studying phonon coherence in diverse solids and provides another metric to interpret broadly used spectroscopies.

ACKNOWLEDGMENTS

We would like to thank Professor Alexander A. Balandin and Professor Fariborz Kargar at the University of California, Riverside for providing us the experimental spectroscopy data. This project is partially supported by the grants from the National Natural Science Foundation of China (Grants No. 11890703, No. 12205220, and No. 12075168), Shanghai Pujiang Program (Grant No. 22PJ1413700), and Science and Technology Commission of Shanghai Municipality (Grants No. 19ZR1478600 and No. 21JC1405600). This work is also supported in part by CREST JST (No. JPMJCR19I1 and No. JPMJCR19Q3). Z.W. is thankful for the support from the Fundamental Research Funds for the Central Universities (Grant No. 22120220556).

[1] M. N. Luckyanova, J. Garg, K. Esfarjani, A. Jandl, M. T. Bulsara, A. J. Schmidt, A. J. Minnich, S. Chen, M. S. Dresselhaus, and Z. Ren, Coherent phonon heat conduction in superlattices, Science **338**, 936 (2012).

[2] J. Ravichandran, A. K. Yadav, R. Cheaito, P. B. Rossen, A. Soukiassian, S. J. Suresha, J. C. Duda, B. M. Foley, C. H. Lee, Y. Zhu, A. W. Lichtenberger, J. E. Moore, D. A. Muller, D. G. Schlom, P. E. Hopkins, A. Majumdar, R. Ramesh, and M. A. Zurbuchen, Crossover from incoherent to coherent phonon scattering in epitaxial oxide superlattices, Nat. Mater. **13**, 168 (2014).

[3] G. Xie, D. Ding, and G. Zhang, Phonon coherence and its effect on thermal conductivity of nanostructures, Adv. Phys.: X **3**, 1480417 (2018).

[4] Z. Zhang, Y. Guo, M. Bescond, J. Chen, M. Nomura, and S. Volz, Coherent thermal transport in nano-phononic crystals: An overview, APL Mater. **9**, 081102 (2021).

[5] M. V. Simkin and G. D. Mahan, Minimum Thermal Conductivity of Superlattices, Phys. Rev. Lett. **84**, 927 (2000).

[6] S. Alaie, D. F. Goettler, M. Su, Z. C. Leseman, C. M. Reinke, and I. El-Kady, Thermal transport in phononic crystals and the observation of coherent phonon scattering at room temperature, Nat. Commun. **6**, 7228 (2015).

[7] S. Hu, Z. Zhang, P. Jiang, J. Chen, S. Volz, M. Nomura, and B. Li, Randomness-induced phonon localization in graphene heat conduction, J. Phys. Chem. Lett. **9**, 3959 (2018).

[8] J. Maire, R. Anufriev, R. Yanagisawa, A. Ramiere, S. Volz, and M. Nomura, Heat conduction tuning by wave nature of phonons, Sci. Adv. **3**, e1700027 (2017).

[9] J. Mendoza and G. Chen, Anderson localization of thermal phonons leads to a thermal conductivity maximum, Nano Lett. **16**, 7616 (2016).

[10] M. N. Luckyanova, J. Mendoza, H. Lu, B. Song, S. Huang, J. Zhou, M. Li, Y. Dong, H. Zhou, J. Garlow, L. Wu, B. J. Kirby, A. J. Grutter, A. A. Puretzky, Y. Zhu, M. S. Dresselhaus, A. Gossard, and G. Chen, Phonon localization in heat conduction, Sci. Adv. **4**, eaat9460 (2018).

[11] T. Juntunen, O. Vänskä, and I. Tittonen, Anderson Localization Quenches Thermal Transport in Aperiodic Superlattices, Phys. Rev. Lett. **122**, 105901 (2019).

[12] R. Hu and Z. Tian, Direct observation of phonon anderson localization in Si/Ge aperiodic superlattices, Phys. Rev. B **103**, 045304 (2021).

[13] Y. Guo, M. Bescond, Z. Zhang, S. Xiong, K. Hirakawa, M. Nomura, and S. Volz, Thermal conductivity minimum of graded superlattices due to phonon localization, APL Mater. **9**, 091104 (2021).

[14] S.-i. Tamura, Y. Tanaka, and H. J. Maris, Phonon group velocity and thermal conduction in superlattices, Phys. Rev. B **60**, 2627 (1999).

[15] W. E. Bies, R. J. Radtke, and H. Ehrenreich, Phonon dispersion effects and the thermal conductivity reduction in GaAs/AlAs superlattices, J. Appl. Phys. **88**, 1498 (2000).

[16] S. K. Gupta and P. K. Jha, Modified phonon confinement model for size dependent Raman shift and linewidth of silicon nanocrystals, Solid State Commun. **149**, 1989 (2009).

[17] F. Kargar, B. Debnath, J. P. Kakko, A. Saynatjoki, H. Lipsanen, D. L. Nika, R. K. Lake, and A. A. Balandin, Direct observation of confined acoustic phonon polarization branches in free-standing semiconductor nanowires, Nat. Commun. **7**, 13400 (2016).

[18] S. Lee, K. Kim, K. P. Dhakal, H. Kim, W. S. Yun, J. Lee, H. Cheong, and J. H. Ahn, Thickness-dependent phonon renormalization and enhanced Raman scattering in ultrathin silicon nanomembranes, Nano Lett. **17**, 7744 (2017).

[19] M. Simoncelli, N. Marzari, and F. Mauri, Unified theory of thermal transport in crystals and glasses, Nat. Phys. **15**, 809 (2019).

[20] L. Isaeva, G. Barbalinardo, D. Donadio, and S. Baroni, Modeling heat transport in crystals and glasses from a unified lattice-dynamical approach, Nat. Commun. **10**, 3853 (2019).

[21] Z. Zhang, Y. Guo, M. Bescond, J. Chen, M. Nomura, and S. Volz, Generalized decay law for particlelike and wavelike thermal phonons, Phys. Rev. B **103**, 184307 (2021).

[22] A. Jain, Multichannel thermal transport in crystalline Tl_3VSe_4, Phys. Rev. B **102**, 201201(R) (2020).

[23] Z. Zhang, Y. Guo, M. Bescond, J. Chen, M. Nomura, and S. Volz, How coherence is governing diffuson heat transfer in amorphous solids, npj Comput. Mater. **8**, 96 (2022).

[24] D. Snoke, *Solid State Physics: Essential Concepts* (Cambridge University Press, Cambridge, UK, 2020).

[25] R. Hu, S. Iwamoto, L. Feng, S. Ju, S. Hu, M. Ohnishi, N. Nagai, K. Hirakawa, and J. Shiomi, Machine-Learning-Optimized Aperiodic Superlattice Minimizes Coherent Phonon Heat Conduction, Phys. Rev. X **10**, 021050 (2020).

[26] P. Jiang, X. Qian, and R. Yang, Time-domain thermoreflectance (TRTR) measurements of anisotropic thermal conductivity using a variable spot size approach, Rev. Sci. Instrum. **88**, 074901 (2017).

[27] J. Zhu, X. Wu, D. M. Lattery, W. Zheng, and X. Wang, The ultrafast laser pump-probe technique for thermal characterization of materials with micro/nanostructures, Nanoscale Microscale Thermophys. Eng. **21**, 177 (2017).

[28] G. S. MacCabe, H. Ren, J. Luo, J. D. Cohen, H. Zhou, A. Sipahigil, M. Mirhosseini, and O. Painter, Nano-acoustic resonator with ultralong phonon lifetime, Science **370**, 840 (2020).

[29] E. Burkel, Phonon spectroscopy by inelastic x-ray scattering, Rep. Prog. Phys. **63**, 171 (2000).

[30] J. Serrano, A. Bosak, R. Arenal, M. Krisch, K. Watanabe, T. Taniguchi, H. Kanda, A. Rubio, and L. Wirtz, Vibrational Properties of Hexagonal Boron Nitride: Inelastic X-Ray Scattering and *Ab Initio* Calculations, Phys. Rev. Lett. **98**, 095503 (2007).

[31] A. J. Minnich, J. A. Johnson, A. J. Schmidt, K. Esfarjani, M. S. Dresselhaus, K. A. Nelson, and G. Chen, Thermal Conductivity Spectroscopy Technique to Measure Phonon Mean Free Paths, Phys. Rev. Lett. **107**, 095901 (2011).

[32] A. Glensk, B. Grabowski, T. Hickel, J. Neugebauer, J. Neuhaus, K. Hradil, W. Petry, and M. Leitner, Phonon Lifetimes throughout the Brillouin Zone at Elevated Temperatures from Experiment and *Ab Initio*, Phys. Rev. Lett. **123**, 235501 (2019).

[33] M. Zacharias, H. Seiler, F. Caruso, D. Zahn, F. Giustino, P. C. Kelires, and R. Ernstorfer, Efficient First-Principles Methodology for the Calculation of the All-Phonon Inelastic Scattering in Solids, Phys. Rev. Lett. **127**, 207401 (2021).

[34] Z. Han, X. Yang, S. E. Sullivan, T. Feng, L. Shi, W. Li, and X. Ruan, Raman Linewidth Contributions from Four-Phonon and Electron-Phonon Interactions in Graphene, Phys. Rev. Lett. **128**, 045901 (2022).

[35] C. Colvard, T. A. Gant, M. V. Klein, R. Merlin, R. Fischer, H. Morkoc, and A. C. Gossard, Folded acoustic and quantized optic phonons in (GaSl)As superlattices, Phys. Rev. B **31**, 2080 (1985).

[36] A. A. Balandin and D. L. Nika, Phononics in low-dimensional materials, Mater. Today **15**, 266 (2012).

[37] J. Cuffe, O. Ristow, E. Chavez, A. Shchepetov, P. O. Chapuis, F. Alzina, M. Hettich, M. Prunnila, J. Ahopelto, T. Dekorsy, and C. M. Sotomayor Torres, Lifetimes of Confined Acoustic Phonons in Ultrathin Silicon Membranes, Phys. Rev. Lett. **110**, 095503 (2013).

[38] R. Nicklow, N. Wakabayashi, and H. G. Smith, Lattice dynamics of pyrolytic graphite, Phys. Rev. B **5**, 4951 (1972).

[39] J. Maultzsch, S. Reich, C. Thomsen, H. Requardt, and P. Ordejon, Phonon Dispersion in Graphite, Phys. Rev. Lett. **92**, 075501 (2004).

[40] J. M. Larkin, J. E. Turney, A. D. Massicotte, C. H. Amon, and A. J. H. McGaughey, Comparison and evaluation of spectral energy methods for predicting phonon properties, J. Comput. Theor. Nanosci. **11**, 249 (2014).

[41] H. Bao, J. Chen, X. Gu, and B. Cao, A review of simulation methods in micro/nanoscale heat conduction, ES Energy Environ. **1**, 16 (2018).

[42] A. J. C. Ladd, B. Moran, and W. G. Hoover, Lattice thermal conductivity: A comparison of molecular dynamics and anharmonic lattice dynamics, Phys. Rev. B **34**, 5058 (1986).

[43] A. J. H. McGaughey and M. Kaviany, Quantitative validation of the Boltzmann transport equation phonon thermal conductivity model under the single-mode relaxation time approximation, Phys. Rev. B **69**, 094303 (2004).

[44] Z. Zhang, S. Hu, T. Nakayama, J. Chen, and B. Li, Reducing lattice thermal conductivity in schwarzites via engineering the hybridized phonon modes, Carbon **139**, 289 (2018).

[45] Z. Zhang, S. Hu, Q. Xi, T. Nakayama, S. Volz, J. Chen, and B. Li, Tunable phonon nanocapacitor built by carbon schwarzite based host-guest system, Phys. Rev. B **101**, 081402(R) (2020).

[46] J. Chen, X. Xu, J. Zhou, and B. Li, Interfacial thermal resistance: Past, present, and future, Rev. Mod. Phys. **94**, 025002 (2022).

[47] Z. Zhang, Y. Guo, M. Bescond, J. Chen, M. Nomura, and S. Volz, Heat Conduction Theory Including Phonon Coherence, Phys. Rev. Lett. **128**, 015901 (2022).

[48] G. P. Srivastava, *The Physics of Phonons* (Routledge, London, 1990).

[49] G. Chen, *Nanoscale Energy Transport and Conversion: A Parallel Treatment of Electrons, Molecules, Phonons, and Photons* (Oxford University Press, Oxford, UK, 2005).

[50] See Supplemental Material at http://link.aps.org/supplemental/10.1103/PhysRevB.107.155426 for (1) normal mode decomposition; (2) mode energy including phonon coherence; (3) direct MD simulations; (4) evaluation of the fitting error; (4.1) definition of the fitting error; (4.2) fitting error for spectroscopy data of GaAs NWs; (4.3) fitting error for spectroscopy data of Si NWs; (4.4) fitting error for spectroscopy data of Si NMs; (5) the fitting of acoustic modes; and (6) thickness-dependent phonon coherence in Si NMs.

[51] The code providing the calculation of phonon coherence and coherence corrected thermal conductivity according to our model as an open-source package WPPT is available at https://github.com/ZhongweiZhangsite/WPPT.

[52] I. F. Crowe, M. P. Halsall, O. Hulko, A. P. Knights, R. M. Gwilliam, M. Wojdak, and A. J. Kenyon, Probing the phonon confinement in ultrasmall silicon nanocrystals reveals a size-dependent surface energy, J. Appl. Phys. **109**, 083534 (2011).

[53] Z. Zhang, Y. Ouyang, Y. Cheng, J. Chen, N. Li, and G. Zhang, Size-dependent phononic thermal transport in low-dimensional nanomaterials, Phys. Rep. **860**, 1 (2020).

[54] K. W. Adu, Q. Xiong, H. R. Gutierrez, G. Chen, and P. C. Eklund, Raman scattering as a probe of phonon confinement and surface optical modes in semiconducting nanowires, Appl. Phys. A **85**, 287 (2006).

[55] S. Plimpton, Fast parallel algorithms for short-range molecular dynamics, J. Comput. Phys. **117**, 1 (1995).

[56] F. H. Stillinger and T. A. Weber, Computer simulation of local order in condensed phases of silicon, Phys. Rev. B **31**, 5262 (1985).

[57] R. Vialla, B. Rufflé, G. Guimbretière, and R. Vacher, Eliminating the broadening by finite aperture in Brillouin spectroscopy, Rev. Sci. Instrum. **82**, 113110 (2011).

[58] B. Latour, S. Volz, and Y. Chalopin, Microscopic description of thermal-phonon coherence: From coherent transport to diffuse interface scattering in superlattices, Phys. Rev. B **90**, 014307 (2014).

[59] P. Martin, Z. Aksamija, E. Pop, and U. Ravaioli, Impact of Phonon-Surface Roughness Scattering on Thermal Conductivity of Thin Si Nanowires, Phys. Rev. Lett. **102**, 125503 (2009).

[60] J. D. Gale, Gulp: A computer program for the symmetry-adapted simulation of solids, J. Chem. Soc. Faraday Trans. **93**, 629 (1997).